

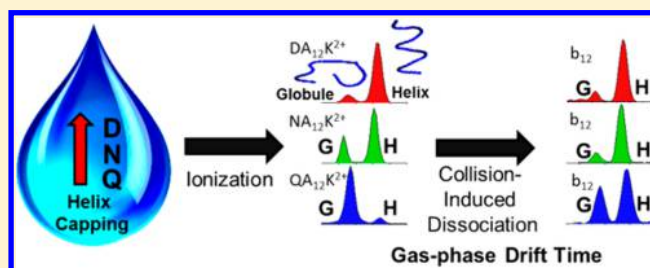
# Gas-Phase Helical Peptides Mimic Solution-Phase Behavior

Lindsay J. Morrison and Vicki H. Wysocki\*

Ohio State University, 484 West 12th Avenue, Columbus, Ohio 43210, United States

**S** Supporting Information

**ABSTRACT:** In solution,  $\alpha$ -helices are stabilized at the termini by a variety of different capping interactions. Study of these interactions in the gas phase provides a unique means to explore the intrinsic properties that cause this stabilization. Evidence of helical and globular conformations is presented here for gas-phase, doubly charged peptides of sequence  $XA_nK$ , wherein X is D, N, Q, or L. The relative abundance of the helical conformation is found to vary as a function of peptide length and the identity of the first amino acid, consistent with solution phase studies that have looked at the identity of the first amino acid. The N-terminal, b ion fragments of the doubly charged precursor peptides are examined as a function of fragment length, N-terminal amino acid, precursor conformation, and the activation energy used to generate the fragment. At lower collision energies, helical b ions preferentially form, particularly from helical precursors. The abundance of the helical b ion population is observed to dramatically decrease for  $NA_n$  and  $DA_n$  b ions smaller than the  $b_{10}$ ; simulations suggest this feature is due to the  $b_{10}$  having two complete turns of the helix, while the  $b_9$  and smaller ions have only a partial second turn, suggesting the  $b_{10}$  is the lower limit for stable helical conformations in b ions. Use of higher collision energies promotes the formation of globular structures in the b ions. This characteristic is attributed to increased conformational dynamics and subsequently improved proton transfer kinetics from the b ion's C-terminal oxazolone ring to the N-terminus.



## INTRODUCTION

The helical content of peptides and proteins determines such biologically relevant behavior as the binding of peptides to drug targets and the interactions of histone tails with DNA. Although the biologically relevant functions of these peptides and proteins occur in solution, gas phase experiments provide a unique means to develop the understanding of the intrinsic structural features that contribute to the relative stability of different  $\alpha$ -helices. One such feature that has been well studied in both the gas and solution phase is acetylation. Acetylation of the N-terminus and lysine side chains has been implicated in a host of biological systems, including histone protein–DNA interactions and T-cell recognition of peptides presented at the cell surface. The biological function of both of these binding interactions has been correlated to conformational changes that occur in the histone tail or peptide following acetylation.<sup>1,2</sup> However, because of the complexity of biological systems, developing an understanding of the conformational effects of acetylation at the molecular level is difficult in a native environment. Gas and solution phase studies of model systems have thus provided insight at the molecular level. Polyalanine helices capped with an N-terminal acetyl group have been known to form stable helices in solution for many years;<sup>3–6</sup> Jarrold and co-workers extended this work to the gas phase, demonstrating that peptides capped with an N-terminal acetyl group and a C-terminal lysine residue form extremely stable helices in the gas phase.<sup>7–12</sup> The gas phase studies suggest that charge plays a critical role in the stability of  $\alpha$ -helices. C-

terminal protonation is stabilized by the helix dipole, while N-terminal protonation destabilizes the helix, resulting in the formation of a globule.<sup>13,14</sup> Blocking the charging at the N-terminus and promoting the formation of an additional hydrogen bond, effected by acetylation, is observed to promote the formation of  $\alpha$ -helices in both the gas and solution phase. Thus, the conformational changes long associated with this particular post-translational modification can be studied relatively directly by use of gas phase experiments, such as ion mobility measurements in a tandem mass spectrometer.

Ion mobility measurements, in conjunction with mass spectrometry, offer an additional dimension of information in the study of gas phase biomolecules, as isomeric structures of a given charge state can often be resolved based on their shape. In conventional ion mobility, a potential gradient is applied to a linear drift cell filled with a helium bath gas. A particular ion will have a drift time ( $t_D$ ) through the cell that is proportional to its collision cross section ( $\Omega$ ) according to the following equation:

$$\Omega = \frac{18\pi^{1/2}}{16} \frac{ze}{(k_B T)^{1/2}} \left[ \frac{1}{M_I} + \frac{1}{M_N} \right] t_D E \frac{760}{L} \frac{T}{P} \frac{1}{273.2 N}$$

where  $z$  is the charge of the ion,  $e$  is the elemental charge,  $k_B$  is Boltzman's constant,  $T$  is the temperature,  $M_I$  is the mass of the ion,  $M_N$  is the mass of the neutral bath gas,  $L$  is the length of

Received: July 18, 2014

Published: September 9, 2014

the drift tube,  $E$  is the electric field,  $P$  is the pressure, and  $N$  is the number density of the neutral gas.<sup>15</sup> Platforms that utilize a traveling wave ion guide to propel ions through the drift gas, as used in the present work, require external calibration methods for the calculation of collisional cross section, and a variety of calibrants suitable for a wide  $m/z$  range have been developed.<sup>16–19</sup> In the present work, IM is used because it provides a useful means, in conjunction with molecular dynamics, to characterize helical vs globular structures of capped peptides and their fragments.

Helical propensity and the stability of helices in the solution and gas phase are of interest from a fundamental perspective but these structures are also of particular interest to the membrane protein community, as helical regions are commonly found in transmembrane domains. Protein complexes with  $\alpha$ -helical transmembrane domains are thought to be relatively stable in the gas phase because of the absence of protic solvents, although these molecules must be transferred into the gas phase via detergents, micelles, or amphipols.<sup>20,21</sup> Modeling and experimental studies in solution have provided extensive information regarding helix propensity as a function of amino acid identity.<sup>3–6,22,23</sup> The majority of these studies, however, have examined helix propensity as a function of amino acid identity in the *interior* of the peptide. The regions that flank the N and C-terminus of the helix, although well studied in solution, have not been examined in the gas phase. Hydrogen bonding with the turn regions adjacent to  $\alpha$ -helices has been shown to be critical in stabilizing the helix.<sup>24–28</sup> The N-terminal end of helices, in particular, are often capped by amino acids that hydrogen bond with the amide hydrogens at the N-terminus of the helix via their side chains.<sup>25,26,28–31</sup> Hydrophobic interactions, however, have also been observed between a residue external to the helix and a residue within the helix.<sup>3</sup> This interaction is thought to shield the exposed amide N–H hydrogen bonding partners at the N-terminus of the helix from solvent interactions. These two restrictions, side chain hydrogen bonding and hydrophobic interactions with the amino acids flanking the N-terminus of  $\alpha$ -helices, limits the number of number of common capping motifs at the N-terminus to approximately three.<sup>24</sup> Interestingly, Aurora and Rose examined over 1000 proteins from the protein data bank and found that hydrophobic capping groups were vastly more common than hydrogen bonding capping groups.<sup>24</sup> In contrast with the crystallography data, a number of solution phase studies have examined helical content as a function of the identity of the N-terminal residue and repeatedly shown that hydrogen bonding residues are preferentially found as the capping residue on the N-terminus of helices. In particular, asparagine and aspartic acid have been shown to provide the greatest stabilizing forces for  $\alpha$ -helices, while nonpolar residues are disfavored at the N-terminal capping position and glutamine is thought to stabilize a nonhelical conformation.<sup>25–27,30,32,33</sup>

Nambiar and co-workers developed the following trend of  $\alpha$ -helix inducing amino acids when placed at the N-terminus: Asp > Asn > Ser > Glu > Gln.<sup>32</sup> The ability of the amide and acid side chains to accept hydrogen bonds from the second and third residues of the helix was found to be essential in the stabilization observed for these residues as capping amino acids. In this study we extend study of helix capping groups to the gas phase, and examine doubly charged helical peptides with an Asp, Asn, Leu, and Gln N-terminal residue. Owing to the lack of solvent, the gas phase is also ideal to examine the absence of

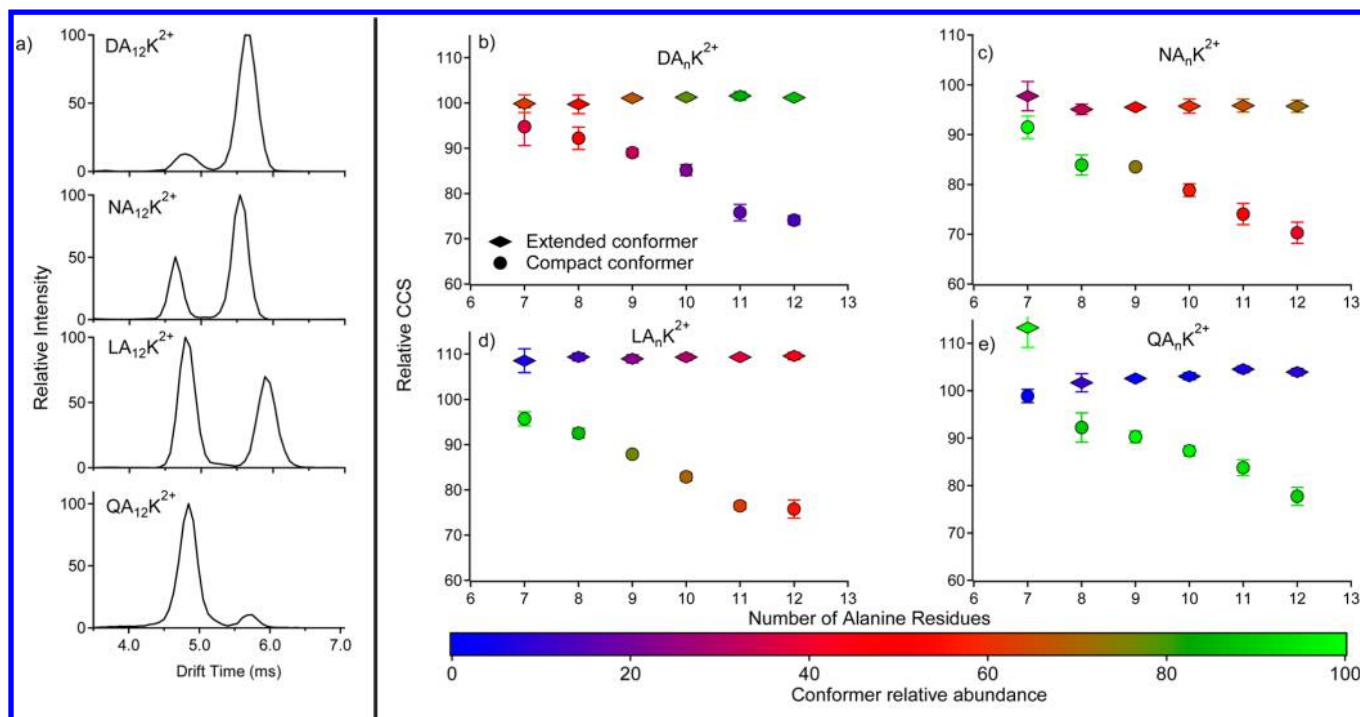
solvent on hydrophobic preferences; we thus examine a leucine-containing peptide in order to compare helix propensity in peptides with a hydrophobic capping residue. Finally, we use ion mobility to characterize the abundance of helices in the N-terminal fragments of the doubly charged precursor peptides. This study addresses different factors such as peptide fragment length, N-terminal amino acid identity, precursor conformation, and collision energy in order to elucidate the stability of  $\alpha$ -helical conformations in gas phase peptide fragment ions. The structure and stability of the fragment ions are probed to better understand the intrinsic stability of capped helices during activation (heating) and whether the abundance of  $\alpha$ -helical fragments is dependent on precursor structure, an element which is of interest to efforts to extend mass spectrometry to the characterization of biomolecule secondary and higher structure.

## EXPERIMENTAL SECTION

Fluorenylmethoxycarbonyl (Fmoc) protected amino acids and synthesis reagents were purchased from Novabiochem (Billerica, MA).<sup>34</sup> Peptides were synthesized in-house using standard solid-phase Fmoc peptide synthesis chemistry as described previously.<sup>34,35</sup> Peptides were cleaved from the resin using 98% trifluoroacetic acid and purified by extraction with diethyl ether and subsequent flash chromatography. XA<sub>n</sub>K polyalanine peptides, where X was either aspartic acid (D), asparagine (N), leucine (L), and glutamate (Q), respectively, were present as mixtures of XA<sub>6</sub>K–XA<sub>13</sub>K and dried under a vacuum prior to dilution into 50:50 acetonitrile:water electrospray solvent.

Ion mobility mass spectrometry experiments were performed on a Waters Synapt G2S TOF mass spectrometer (Manchester, UK). Peptides were introduced into the gas phase via a custom nanoelectrospray source in which a glass capillary tip with an approximately 1–10  $\mu\text{m}$  aperture, filled with the peptide solution, was fitted over a platinum wire. Nanospray was accomplished by the application of 1–1.5 kV to the platinum wire. Doubly charged precursor peptides were mass selected by the quadrupole prior to activation (6–18 V) and ion mobility analysis. The pressure in the trap collision cell was  $(2–4) \times 10^{-2}$  mbar and the pressure in the transfer TWIG was typically  $(1–2) \times 10^{-2}$  mbar. Typical drift cell pressures were 5–10 mbar, typical wave heights were 18–25 V, and typical wave velocities were 300–650 m/s. Helium gas, which was used for collisional cooling between the CID cell and the IM cell, was introduced at a flow rate of 180 mL/min. Experimental collisional cross sections (CCS) were obtained using singly and doubly charged DL-polyalanine peptides (SigmaAldrich, St. Louis, MO) as a calibration mixture using the collisional cross section database published by Bush et al.<sup>36</sup> Drift time measurements were collected in triplicate, on separate days, and the abundance of the drift time populations was calculated by manually fitting Gaussian curves to the drift time distributions. The area of the Gaussian curves was integrated and error bars generated from the triplicate treatments.

Molecular dynamics simulations were carried out using the Amber-Cornell force field in the NAMD software.<sup>37</sup> Ab initio computations were performed using the Gaussian09 software suite. Geometry optimizations and energy calculations were performed on N-terminally acetylated (neutral and protonated) AlaAla oxazolone dipeptides using the B3LYP/6-31G\* basis set.<sup>38</sup> The bond lengths, angles, and torsional angles from the lowest energy structures were used to generate topology and parameter files for AlaAla oxazolone residues, which were treated as a single C-terminal amino acid in the topology file. Molecular dynamics (MD) simulations were performed at 300 K and were carried out for 10 ns. Starting structures were linear, unstructured b ions terminated with an oxazolone ring and were constructed using the GaussView03 program.<sup>38</sup> Simulated annealing was performed by heating and cooling the peptides in 50K increments from 250 to 900 K or 1250 K. The globular, but oxazolone protonated, b<sub>12</sub> ion from NA<sub>12</sub>K was used as the starting structure in this



**Figure 1.** (a) Drift time distributions of doubly charged  $DA_{12}K^{2+}$ ,  $NA_{12}K^{2+}$ ,  $LA_{12}K^{2+}$ , and  $QA_{12}K^{2+}$ , showing the presence of both an extended and a compact conformer, the relative abundance of which varies with the identity of the first amino acid. The relative collisional cross sections ( $\Omega = 14.5 \times \#ala$ ) of (b)  $DA_nK^{2+}$ , (c)  $NA_nK^{2+}$ , (d)  $LA_nK^{2+}$ , and (e)  $QA_nK^{2+}$  peptides is shown as a function of  $n$ , the number of alanine residues. The relative abundances of the extended and compact conformations are denoted by the color of the marker, with blue corresponding to low abundance, red to intermediate abundance, and green corresponding to high abundance.

simulation. Predicted collisional cross sections were obtained using the coordinates from the MD simulations and the MOBCAL program.<sup>15,39</sup> Reported CCS values were obtained from the trajectory method calculation, which is considered the most accurate method for calculating CCS for small and medium-sized molecules.<sup>15,39</sup> This method for determining CCS from atomic coordinates differs from the other two algorithms included in the MOBCAL software by its inclusion of long-range attractive potentials between the ion and the buffer gas.

## RESULTS

**Ion Mobility of  $XA_nK^{2+}$  Peptides.** Although the bulk of eukaryotic and yeast proteins are acetylated at the N-terminus, many lack this modification. Under physiological conditions, the N-terminus of peptides and proteins lacking an acetyl group is often protonated. The majority of all gas phase studies examining helical model systems, however, have focused on N-terminally acetylated systems.<sup>12–14,40</sup> Relatively short, N-terminally acetylated and C-terminally capped polyaniline peptides ( $n = 7–15$ ) have been shown to be  $\alpha$ -helical in the gas phase and longer nonacetylated polyaniline peptides ( $n = 20–30$ ) have been shown to feature small to moderate helical populations, however, the minimal length for which non-acetylated polyaniline peptides are stable in the gas phase has not been probed. Moreover, the structure of peptides protonated at both the N-terminus and the C-terminal lysine is unclear. In order to investigate the stability of doubly charged polyaniline peptides, polyaniline peptides of moderate length (8–15 residues) and containing a C-terminal lysine cap and a free N-terminus were synthesized. Aspartic acid and asparagine were used as the N-terminal amino acid because they have been shown in the solution phase to stabilize  $\alpha$ -helices when used as an N-terminal cap, while glutamine was used because it

stabilizes a nonhelical structure. Leucine was used for comparison as a hydrophobic amino acid of approximately the same mass but having no side chain hydrogen bonding capabilities.

Mass spectrometry and ion mobility analyses were performed on doubly charged  $NA_nK$ ,  $DA_nK$ ,  $QA_nK$ , and  $LA_nK$ , where  $n$ , the number of alanine residues, was varied from 7 to 12. Figure 1(a) shows representative drift time distributions for the  $XA_{12}K^{2+}$  peptides, from which it can be seen that the relative abundance of the compact and extended conformations changes as a function of the identity of the first residue. The drift time distributions of all four peptides are bimodal, with each of the doubly charged peptides having both an extended and compact conformation. In doubly charged  $DA_{12}K$ , the extended drift time population is dominant and comprises approximately 90% of the total population. The relative abundance of this conformation is reduced in the  $NA_{12}K^{2+}$  and  $LA_{12}K^{2+}$  peptides ( $\approx 70$  and  $40\%$ , respectively), and is significantly reduced in the  $QA_{12}K^{2+}$  peptide, which features only 10% of the extended conformer. Comparison of the  $QA_{12}K^{2+}$  peptide with the  $DA_{12}K^{2+}$  and  $NA_{12}K^{2+}$  peptides suggests that the extended conformation in the Asn and Asp-containing peptides is stabilized by interactions involving gamma-branched amide/acid side chains capable of H-bonding but not by the similar delta-branched amide side chain. Comparison of the relative abundance of the compact and extended conformations in  $NA_{12}K^{2+}$  and  $QA_{12}K^{2+}$  peptides is also particularly interesting; although the peptides differ only by a single methylene group in the side chain of the first amino acid, the relative abundance of the extended conformation changes from 70 to 10%. The difference in the relative abundance of these two conformations in these two peptides

suggests that the length of the side chain of the N-terminal amino acid plays a critical role promoting particular conformations of the peptide. The peptide with a hydrophobic, branched N-terminal amino acid, LA<sub>12</sub>K<sup>2+</sup>, has an intermediate abundance of the extended and compact conformations, suggesting that the absence of hydrogen bonding partners at the N-terminus destabilizes the extended conformation relative to the peptides containing gamma-branched amino acids that can H-bond.

Collisional cross sections ( $\Omega$ ) were calculated from the drift times and subsequently converted into relative CCS ( $\Omega_{\text{rel}}$ ).<sup>16</sup> Jarrold and co-workers have proposed using plots of relative collisional cross section as a function of the number of alanines as a means to determine if a peptide series is helical. Relative CCS is given by  $\Omega_{\text{rel}} = \Omega - 14.5n$ , where  $n$  is the number of alanine residues and 14.5 is the CCS of a single alanine in an  $\alpha$ -helix.<sup>41</sup> Thus, plots of relative CCS against the number of alanine residues generate horizontal trends for  $\alpha$ -helical series of peptides, and trends with negative slopes for globular peptides. Figure 1(b–d) show the relative CCS of the extended and compact conformations of the XA<sub>*n*</sub>K<sup>2+</sup> peptides as a function of the number of alanine residues in the peptide. In some cases the error bars are not visible because they are smaller than the marker. It should be noted that the relative abundance of the compact and extended distributions was not observed to change upon activation (4–50 eV), suggesting that the observed drift time distributions represent gas phase equilibrium. Inspection of Figure 1(b–e) shows that the relative CCS of the extended conformations of the XA<sub>*n*</sub>K<sup>2+</sup> peptides follow horizontal trends, suggesting that the extended conformation is  $\alpha$ -helical. In contrast, the relative CCS of the more compact conformations have a negative slope, suggesting that these conformers have a more globular secondary structure. This is in good agreement with the work of Jarrold and co-workers with polyalanine and Aca<sub>*n*</sub>K systems, in which the more extended conformers were  $\alpha$ -helical.<sup>40</sup>

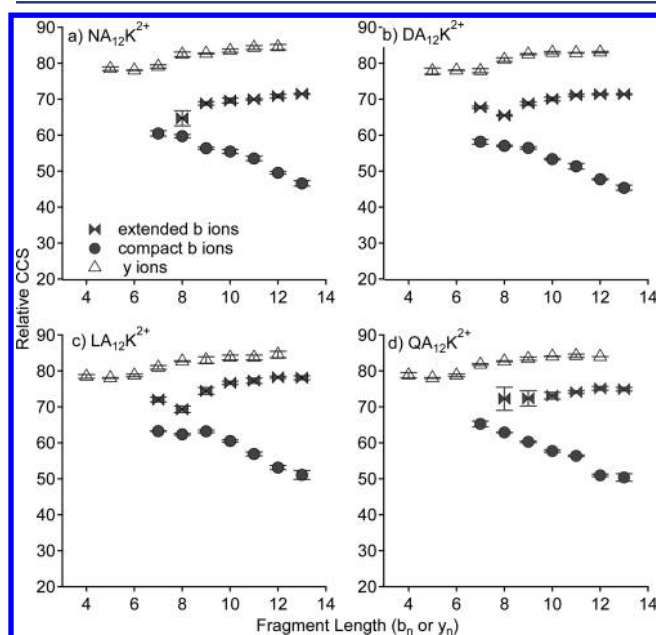
The relative abundance of the extended and compact conformations were calculated by fitting and manually parametrizing Gaussian distributions to the experimental drift time distributions. Gaussian functions were of the form:  $G_{\text{fit}} = a \times e^{-(t_0 - b)^2 / (2c^2)}$ , where  $a$ , the height of the curve,  $b$ , the center of the distribution, and  $c$ , width of the distribution were fit to each drift time distribution. The area,  $A$ , of the curve was calculated by integrating the function across all space, which simplifies to  $A = ac\sqrt{\pi}$ . The color of the markers in Figure 1 reflects the intensity of the helical and globular conformations, normalized to the summed area of both distributions. From this plot it is clear that the relative abundance of the  $\alpha$ -helical population decreases with the decreasing length of the peptide. Although this effect is less pronounced in the QA<sub>*n*</sub>K<sup>2+</sup> and NA<sub>*n*</sub>K<sup>2+</sup> series, it is nonetheless still present. The helical population is a minor population for all peptides smaller than XA<sub>9</sub>K<sup>2+</sup>, although it is present to some extent in the DA<sub>7</sub>K<sup>2+</sup>, DA<sub>8</sub>K<sup>2+</sup>, and NA<sub>8</sub>K<sup>2+</sup> peptides. Thus, the lower limit for the formation of helical structures for these doubly charged peptides, although dependent on the identity of the N-terminal amino acid, is approximately 7–9 residues. The stabilizing effect of the N-terminal amino acid on the helical structure of is in excellent agreement with the solution phase work performed independently by Baldwin and Nambiar, suggesting that certain structural features of peptides, such as helical capping groups, are independent of the gas or solution phase environment. It is

appealing to consider this result in the context of the gas phase peptides having a “memory” of their solution phase conformations. However, the absence of change in the relative abundance of the helical and globular conformations upon activation suggests that the measured populations have already reached gas phase equilibrium. It is therefore likely that the gas phase behavior of N-terminal capping group mimics the solution phase behavior rather than being a direct carry over from it. Unfortunately, we were unable to measure the solution equilibria because the peptides were present as complex mixtures of different chain lengths.

The QA<sub>7</sub>K<sup>2+</sup> and LA<sub>10</sub>K<sup>2+</sup> peptides both feature unusual drift time distributions, as the leucine peptide contains what appears to be several globular subpopulations (see Supporting Information Figure S1) and the relative abundance of the extended conformation of QA<sub>7</sub>K<sup>2+</sup> is of greater abundance than the extended conformation of all other Gln-containing peptides. Although interesting, the particular intramolecular interactions that contribute to these anomalies is beyond the scope of this paper. It should additionally be noted that peptides smaller than XA<sub>7</sub>K<sup>2+</sup> were not included in this study because the difference in CCS between the extended and compact conformers was not large enough to be resolved by the ion mobility instruments used. Despite this, it is possible to extrapolate decreasing population abundances to get a rough lower limit for the four peptide series as the decline in helical abundance follows a linear relationship (LA<sub>*n*</sub>K<sup>2+</sup>, NA<sub>*n*</sub>K<sup>2+</sup> and DA<sub>*n*</sub>K<sup>2+</sup> series). A population abundance of greater than or equal to 10% of the total population will be used as the “lower limit” of stability of the helical conformation. By this criterion, the lower limit for the leucine-containing peptides is the LA<sub>8</sub>K<sup>2+</sup> peptide. Classification of the glutamine-containing peptides is inherently difficult owing to the abundance of the helical conformation being less than 10% for all of the larger peptides. As noted above, a larger extended population is present for the QA<sub>7</sub>K<sup>2+</sup> peptide, which is likely due to the presence of a different structure, owing to the anomalous CCS and intensity of this species. By extrapolation of the decreasing abundance of the NA<sub>*n*</sub>K<sup>2+</sup> and DA<sub>*n*</sub>K<sup>2+</sup> populations, the lower limit for the helical conformation in these systems can be estimated to be the NA<sub>6</sub>K<sup>2+</sup> and the DA<sub>5</sub>K<sup>2+</sup> peptides. It is possible that this method overestimates the stability of the asparagine- and aspartic acid-containing peptides, however, as it is possible that the stability of the helical conformation could fall off very rapidly.

**IMS of the b Ion Fragments of XA<sub>12</sub>K<sup>2+</sup>.** Cleavage of amide bonds in peptides by CID activation has been studied extensively.<sup>35,42–51</sup> Although a variety of mechanisms exist, the oxazolone pathway is thought to dominate in most cases. By this pathway, nucleophilic attack of the preceding carbonyl oxygen on the carbonyl carbon of any given amide bond yields a five-membered ring oxazolone b ion as the N-terminal fragment and a linear y ion as the C-terminal fragment.<sup>43,52</sup> In contrast to the exhaustive work that has been performed examining the structures of b ions, the secondary structures of larger b ions are much less well understood. A recent publication by Russell and co-workers has shown using 2D ion mobility–mass spectrometry plots that it is possible to rapidly determine helical and globular b and y ions based on the slope of the trend line.<sup>53</sup> However, the molecular basis for the formation and stability of helical fragment ions has not been defined. We hypothesize that b ions of a particular length and with certain N-terminal capping residues will have helical

secondary structures and used the  $\text{XA}_{12}\text{K}^{2+}$  peptides as models to investigate the conformations of these fragment ions, the minimum length at which a helical b ion may occur, and whether or not the conformation of a particular b ion is related to the precursor conformation. Peptides were activated by collision induced dissociation (CID) and then analyzed by IM-MS. Relative collisional cross sections of the fragment ions formed from the  $\text{XA}_{12}\text{K}^{2+}$  peptides by using an activation energy of 36 eV are shown in Figure 2. The y ions form a single



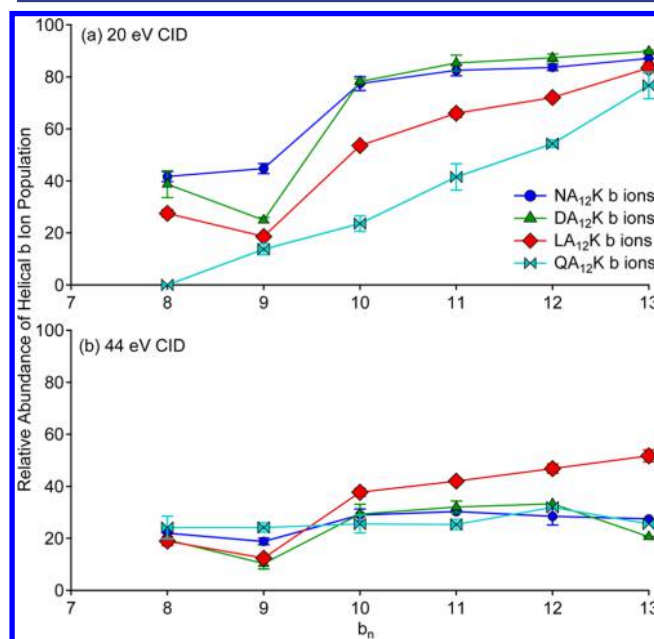
**Figure 2.** Relative CCS of the singly charged b and y ions from (a)  $\text{NA}_{12}\text{K}$ , (b)  $\text{DA}_{12}\text{K}$ , (c)  $\text{LA}_{12}\text{K}$ , and (d)  $\text{QA}_{12}\text{K}$ .

drift time distribution and the b ions form bimodal drift time distributions. The relative CCS of the y ions follows an approximately horizontal trend as a function of the number of alanine residues in the fragment, suggesting they have a helical structure. The average relative CCS, however, changes between the  $y_6$  and  $y_7$ , suggesting the structure of the y ions changes at the  $y_7$  or  $y_8$  ion, presumably from small globules to helices. All equivalent y ions, that is, the same  $y_n$  from each of the four different precursors, have the same CCS. This suggests that the observed y ion population is the gas phase equilibrium conformation and forms independently of the structure of the precursor peptide.

The drift time distributions of the larger b ion fragments are bimodal and feature compact and extended populations similar in appearance to the precursor peptides. The relative CCS of the b ions is plotted as a function of the fragment ion length in Figure 2. The relative CCS of the compact and the extended b ion conformations have a generally downward and relatively horizontal trend, respectively, suggesting that the extended population is helical and the compact globular. This assignment is supported by the relative abundance of the extended and globular b ions as a function of ion length. The relative abundance of the extended population decreases with decreasing b ion length, which is consistent with the extended population being helical, as shorter helical ions are expected to be less stable. It should be noted that the  $b_8$  species falls off the line in all extended b ion series and suggests that this b ion may have a different structure. Therefore, we tentatively assign the

extended  $b_n$  ion population ( $n \geq 9$ ) and the  $y_n$  ion population ( $n \geq 8$ ) to have helical conformations. This assignment is supported by molecular dynamics simulations, which are discussed in more detail below.

In order to illustrate the relative abundance of the helical and globular b ions as a function of fragment length, the helical b ion conformation formed from the  $\text{XA}_{12}\text{K}^{2+}$  peptides is plotted in Figure 3 as a function of the fragment length of the b ion.

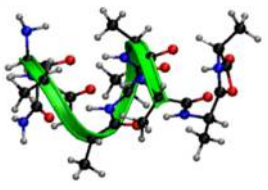
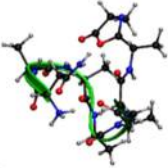
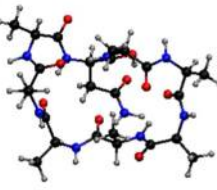
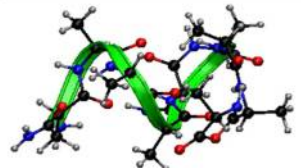

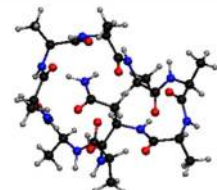
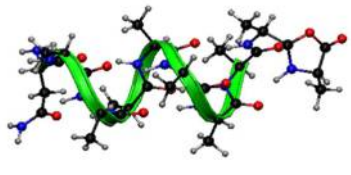

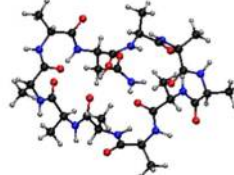
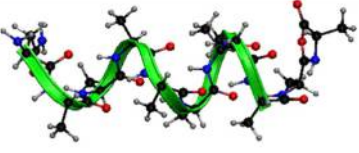
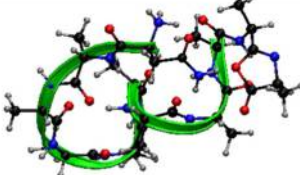

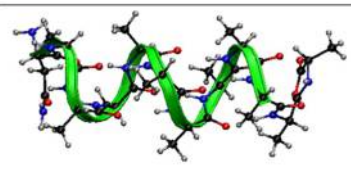
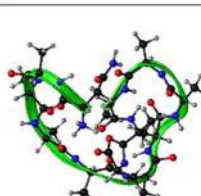
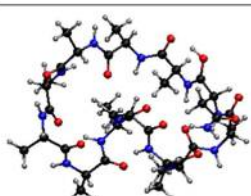
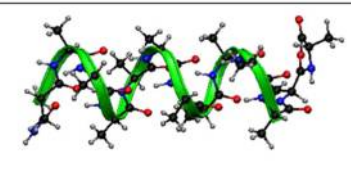
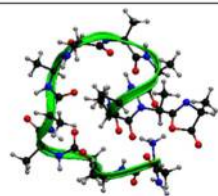
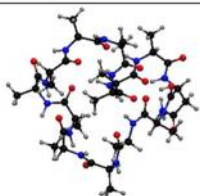


**Figure 3.** Relative abundance of the helical b ion population from  $\text{NA}_{12}\text{K}^{2+}$ ,  $\text{DA}_{12}\text{K}^{2+}$ ,  $\text{LA}_{12}\text{K}^{2+}$ , and  $\text{QA}_{12}\text{K}^{2+}$  using (a) 20 eV and (b) 44 eV collision energies.

The globular population is simply 100 minus % helical (not shown). The helical b ions are plotted following activation at 20 and 44 eV, which represent the lower and higher energy regimes of the peptides as the precursor peptides are approximately 5 and 90% dissociated, respectively, at these energies. Several features of these plots are instructive. Comparison of the plots in (a) and (b) shows that the relative abundance of the globular and helical b ion conformers strongly depends on collision energy. Both Figure 3(a) and Figure 3(b) also show that the stability of the extended conformation varies as a function of the identity of the first residue. At low collision energies, the aspartic acid- and asparagine-containing fragments have the largest relative abundance of the helical conformation, the leucine-containing fragments have intermediate abundances of the helical conformation, and the glutamine-containing fragments have the lowest abundance of the helical conformation. This is the same pattern that was observed in the precursors (see Figure 1) and suggests that there is a correlation between the conformations of the precursor ions and the conformations of the b ions from that precursor.

For all b ions, as the length of the fragment decreases, the relative abundance of the helical population decreases and the abundance of the globular population increases. However, the trend for this relationship depends on the identity of the first residue. In the lower energy regime, the relative abundance of the helical conformation in the  $\text{DA}_n$  and  $\text{NA}_n$  b ions remains relatively constant for  $b_{10}$ – $b_{13}$  ( $\text{Ala}_9$ – $\text{Ala}_{12}$ ) and then decreases dramatically from the  $b_{10}$  to the  $b_9$  ions, by 33% in the  $\text{NA}_n$

Table 1. Representative Frames from MD Simulations of Linear  $NA_n$   $b_8$ – $b_{13}$  Ions Protonated on the Oxazolone Ring, the N-Terminus, and Macrocyclic Structures

	Oxazolone protonated	N-terminus protonated	Macrocyle
$b_8$			
$b_9$			
$b_{10}$			
$b_{11}$			
$b_{12}$			
$b_{13}$			

series and by 50% in the  $DA_n$  series. In contrast, the relative abundance of the  $QA_n$  helical b fragments decreases linearly with the peptide length and the  $LA_n$  series behaves intermediate to the  $QA_n$  and  $D/NA_n$  fragments, exhibiting both a linear decrease in helical content and a sharp drop at the  $b_9$  ion. In contrast, in the higher energy regime, all peptides with a polar first residue, the  $DA_n$ ,  $NA_n$ , and  $QA_n$  series, have a relatively constant 22–30% helical population. This is particularly striking as the relative abundance of the helical species at this energy seems to be less dependent on fragment length than at

the lower collision energy. The  $LA_n$  b ions exhibit largely the same trend as they did at low energies, having both a linear decrease in the relative abundance of the helical b ion as the length of the fragment decreases but also featuring a drop in helix abundance between the  $b_{10}$  and  $b_9$  ions. In order to understand the behavior of the peptide at high and low energies, it is necessary to consider the structure of the b ion fragments.

The behavior of the  $XA_n$  b ions can be rationalized by considering the protonation site of the b ion and the

**Table 2. Experimental and Computed Collisional Cross Sections Based on an Average of 20 Frames from MD Simulations of the  $b_{8-13}$  Ions from  $NA_{12}K^a$** 

	TJM CCS ( $\text{\AA}^2$ )			experimental CCS ( $\text{\AA}^2$ )	
	oxazolone protonated helix	N-terminally protonated globule	macrocycle	extended conformation	compact conformation
$b_{13}$	245.2 (-75.8)	239.1 (-177.2)	231.5	245.5	220.6
$b_{12}$	231.3 (-54.7)	216.4 (-173.8)	220.7	230.4	209.0
$b_{11}$	216.4 (-62.5)	205.3 (-147.9)	208.5	215.0	198.5
$b_{10}$	201.5 (-50.6)	188.3 (-148.6)	198.4	200.1	186.0
$b_9$	187.5 (14.4)	181.5 (-150.8)	182.5	184.8	172.4
$b_8$	173.1 (-34.3)	161.4 (-138.8)	166.3	166.2	161.2

<sup>a</sup>The relative energies of the helical and globular b ions are shown in parentheses (kcal/mol).

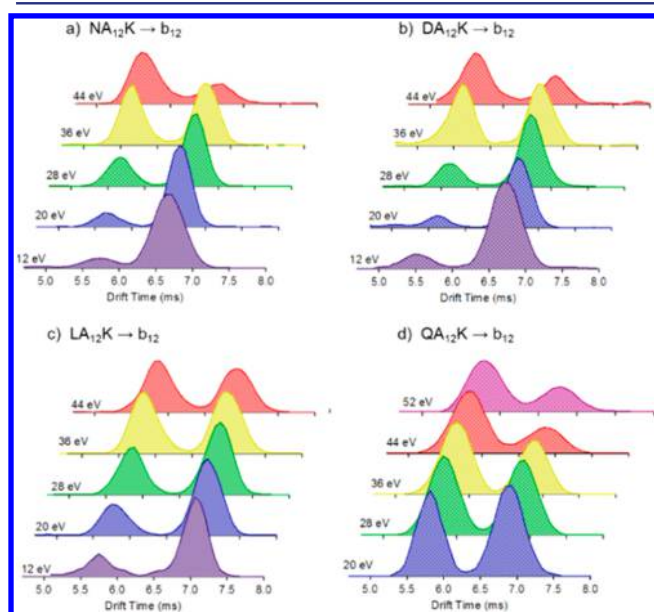
conformation of the precursor. Jarrold and co-workers have demonstrated with precursor peptides that an N-terminal lysine residue destabilizes the gas-phase helical structure while a C-terminal lysine residue stabilizes gas phase helices.<sup>40</sup> Protonation on the C-terminal oxazolone ring of a b ion thus is predicted to stabilize the helical conformation while protonation at the N-terminus is predicted to destabilize the helical conformation. Protonated and neutral oxazolone structures are shown in Supporting Information Figure S2. To explore the effect that protonation site has on the conformation of the b ions, molecular dynamics simulations (3–5 ns), using the Amber–Cornell force field and the NAMD and VMD softwares, were performed on the oxazolone and N-terminally protonated  $NA_n$   $b_{8-13}$  ions.<sup>54</sup> The  $b_{8-13}$  fragment ions protonated on the C-terminal oxazolone ring minimized to  $\alpha$ -helices very rapidly, typically on the picosecond time scale. All N-terminally protonated peptides minimized to globular structures in which the N-terminus was either solvated by head-to-tail interactions with the oxazolone ring carbonyl oxygen or by interactions with the amide backbone. Representative frames from these simulations are shown in Table 1. Starting structures were linear, unstructured peptides. It is conceivable, however, that the compact b ions have macrocycle structures caused by nucleophilic attack of the N-terminus on the oxazolone ring and subsequent isomerization, which has been shown to occur for  $b_4$ – $b_8$  ions.<sup>47</sup> To differentiate between a globule (conformational isomer of an  $\alpha$  helix) and a macrocycle (structural isomer), annealing simulations were performed on  $b_n$  macrocycles. The cyclic structures were generated in GaussView and were heated and cooled from 300 to 900 K and back to 300 K in order to find the lowest energy conformation of the ring. For simplicity only protonation on the asparagine carbonyl oxygen was considered.

Representative frames (20) from the equilibrated structures were input into the MOBCAL program and the average CCS of the 20 frames calculated by the trajectory method (TJM).<sup>15</sup> Table 2 summarizes these cross sections, the experimentally determined cross sections, and the relative energies of helical and globular b ions based on the average energy over 50 frames of the stabilized conformations from the MD simulations. The reported energy is relative to the linear, unstructured peptide in all cases. Good agreement is seen between the extended drift time distribution and the helical conformations (oxazolone protonated) and somewhat good agreement observed between the compact drift time distributions and the N-terminally protonated, globular conformations. In general, the predicted collisional cross sections of the globular species are higher than measured experimentally and it is therefore possible that the precise conformation of the globules is not correct. Because the conformational freedom of globules is expected to be higher

than helices, it is possible that the compact population is a mixture of interconverting species. It is also possible that the compact structure is a globule with the charging proton solvated by multiple carbonyl oxygens. The macrocycle structures were generally similar but slightly larger in collisional cross section than the predicted globular structures, making it difficult to assign one structure vs the other based on predicted CCS alone. It should be noted that the typical accuracy of cross sections obtained from measurement on a TWIMS platform with  $N_2$  as the bath gas are typically within 2% of values measured using traditional platforms; in contrast, the accuracy of the trajectory method for calculating CCS is generally poorer and can be as high as 5–8%.<sup>55–57</sup> Considering the  $NA_{12}$   $b_{13}$  ion, this is equivalent to roughly 12–20  $\text{\AA}^2$ . Given the extended and compact  $NA_{12}$   $b_{13}$  distributions differ in CCS by only 25  $\text{\AA}^2$ , this raises a question regarding the assignments of the helix and globule/macrocycle. A study, in which experimental and computationally derived collisional cross sections were compared for tripeptide systems, investigated this issue directly and showed poor correlation between the trajectory method computed cross sections and experimentally derived cross sections, with the trajectory method values being different from the experimental values by approximately 8%.<sup>58</sup> Zakharova et al.'s concern regarding this error, however, was offset by the predicted cross sections following the same relative trends as the structurally isomeric tripeptides. In the present study, the helical conformations were consistently predicted to have larger cross sections than the globular/macrocycle conformations, which lends support to the assignments. Moreover, the agreement observed between the cross sections predicted for the helical conformation and those found experimentally for the extended distribution provides compelling evidence to suggest the accuracy of the trajectory method is reasonably good for the helical conformations. It should be noted that CCS values measured in  $N_2$  but converted to He numbers via calibration is common practice in the field and generally produces accurate values. However, this conversion is under examination by other groups and it is conceivable that significant errors could exist. Clearly, differentiating between the macrocycle and globule structures on the basis of CCS alone is impossible. However, because macrocyclic structures have been shown to generally form minor populations for larger b ions, it is unlikely that the compact  $b_8$ – $b_{13}$  conformations are macrocyclic.<sup>47</sup> Molecular dynamics simulations support the assignment of the extended drift time distribution as an oxazolone protonated  $\alpha$ -helical b ion. On the basis of simulations, the compact drift time distribution could be an N-terminally protonated globular b ion or macrocycle. For simplicity, we assign the compact population to be globular,

but note that a minor macrocyclic population may exist in the compact arrival time distribution.

The relationship between the observed b ion structure and the collision energy was investigated by increasing the collision energy in small intervals and examining the resulting drift time distribution of the  $b_{12}$  ion. Figure 4 shows the drift time



**Figure 4.** Drift time distributions of the  $b_{12}$  from (a)  $NA_{12}K$ , (b)  $DA_{12}K$ , (c)  $LA_{12}K$ , and (d)  $QA_{12}K$  following dissociation at a series of increasing collision energies.

distributions of the  $b_{12}$  fragment of doubly charged  $NA_{12}K$ ,  $DA_{12}K$ , and  $LA_{12}K$  following activation at 12–44 eV and of doubly charged  $QA_{12}K$  following activation at 20–52 eV. Higher energies were used for the  $QA_{12}K^{2+}$  peptide because it is slightly higher in mass and requires more energy to fragment equivalently by the same fractional reduction in precursor. The globular conformation of all  $b_{12}$  ions smoothly increases in relative abundance as collision energy is increased, consistent with it being more stable or entropically favorable. The distribution of globule and helix following activation at 44 eV in the aspartic acid, asparagine, and glutamine-containing fragments is very similar ( $\approx 70:30$ ) at higher energy, suggesting that the precise chemistry of polar side chains is less important to the stability of helical and globular b ion structures than is the mere presence of a polar functionality in this energy regime. In contrast, the leucine-containing b ion fragment is observed to have a roughly equal distribution of globular and helical conformations following activation at 44 eV. Because leucine lacks a polar side chain, proton shuttling, facilitated by the side chain of the N-terminal amino acids with H-bonding capabilities, may be implicated by these plots. Proton transfer from the protonated oxazolone ring to the N-terminus may therefore occur with assistance from the side chains of the amino acids at the N-terminus.

## DISCUSSION

In the context of capping amino acids, the results presented here are in good agreement with solution phase studies presented separately by Baldwin and Nambiar.<sup>27,32</sup> We observe the same capping group stabilization of the helix, wherein aspartic acid is more stabilizing than asparagine, and glutamine

is more destabilizing. Interestingly, although Aurora and Rose observed a greater prevalence of alpha helices with hydrophobic capping than hydrogen-bonding capping in crystalline proteins, we find that the relative abundance of the helical population in the leucine-containing peptide is less than the relative abundance of the helical population in the aspartic acid and asparagine containing peptides.<sup>24</sup> This suggests that gas-phase hydrogen bonding exerts a greater capping group stabilization than does hydrophobicity. By extension to the solution phase, this would indicate that solvent influence is critical to the stabilization caused by hydrophobic capping groups. It is interesting to note that the glutamine capped peptides, although capable of hydrogen bonding, form the least abundant helical population. One explanation for this behavior is that the glutamine side chain may stabilize a nonhelical conformation such as the globule, as has been shown in solution phase studies.<sup>25,26</sup> Thus, the order of N-terminal capping residue stabilization,  $D > N > L > Q$ , observed in this study is the result of side chain stabilization of the helical conformation by certain amino acids and stabilization of presumably the globular conformation by others.

It has been suggested that the hydrogen bonds responsible for holding together the secondary structures of molecules are broken during ion activation, leading to a “melting” of secondary structure.<sup>59,60</sup> This effect undoubtedly has a threshold, however. It is conceivable, for example, that activation at low energies would result in some hydrogen bonding interactions being broken, but others retained. This is particularly true for fragment ions of substantial length; hydrogen bonds near to the site of fragmentation are certainly disrupted while interactions more remote from the fragmentation site may remain intact. This can be loosely thought of as “local melting” or fraying and we hypothesize that this may occur in larger peptides, particularly when activated using relatively low collision energies. In smaller systems, although all hydrogen bonds may be broken, the relative time scales of fragmentation and rearrangements may permit the fragment ions to retain some of the characteristics of the precursor. For example, if the time scale of fragmentation is much faster than the time scale of conformational changes in the entire fragment backbone, which is reasonable in most cases, it is conceivable that a helical peptide could retain a more elongated shape during activation while a globule could retain a more compact shape. Thus, at low activation energies, the proximity of the N-terminus to the oxazolone ring in the subsequent b ion may be related to the secondary structure of the precursor peptide. In predominantly helical peptides such as  $NA_{12}K^{2+}$  and  $DA_{12}K^{2+}$ , this would result in the N-terminus of the b ion being quite far from the oxazolone immediately following fragmentation.

We have shown using molecular dynamics simulations that N-terminally protonated b ions form globular structures that are more stable than their oxazolone protonated, helical counterparts. Immediately following cleavage of the backbone amide bond, the charging proton is located on the C-terminal oxazolone ring of the b ion and two major processes can occur: conformational rearrangement and/or proton transfer of the proton to the N-terminus or other basic site. These processes are competitive but also codependent, as the conformation of the b ion immediately following ring closure directly impacts the proton transfer events that can occur and how fast they can occur. Although proton transfer can occur on a picosecond time scale and rearrangement on a nanosecond time scale, proton transfer is rate-limited by requiring the molecule to be



in an orientation conducive to the transfer. Thus, a b ion in which the N-terminus and C-terminal oxazolone are in close proximity is significantly more likely to have direct and immediate proton transfer from the C-terminus to the N-terminus than a b ion in which the termini are separated in space, e.g., helical/rod-like in space. It is also possible that protons can migrate by shuttling along the amide backbone; this is expected to be considerably slower, however, because of the number of shuttling events and disruption of helix that would need to occur. More elongated b ions that result from the fragmentation of helical peptides are predicted to have the oxazolone ring and N-terminus remote in space while more compact b ions are more likely to have conformations in which the two termini are proximal. Consequently, the rate at which C- to N-terminal proton transfer can occur in b ions generated from helical precursors is expected to be low, permitting the b ion to remain in, or fold into, a helix. This is consistent with our observation that helical b ions are typically formed from helical precursors. In contrast, the rate of proton transfer between the oxazolone ring and N-terminus in b ions from globular precursors is expected to be much higher, if a conformation in which two termini interact is present. If a hydrogen bond does not form between the two termini and the rate of proton transfer in the compact b ion population is sufficiently slow, conformational rearrangement of the peptide backbone may dominate and a helical b ion could form.

To test this hypothesis, simulated annealing was performed on the  $NA_{11}$  b<sub>12</sub> ion. An oxazolone protonated, globular b<sub>12</sub> ion was used as the starting structure and was heated in 50 K increments from 250 to 1250 K over 2 ns and the temperature of the system subsequently reduced in 50 K increments from 1250 to 300 K over another 2 ns. The equilibrated structures from this treatment were  $\alpha$ -helical b ions, which is consistent with this conformation being the most stable for the oxazolone ring protonation site (but less stable than the N-terminally protonated globule). The starting and equilibrated structures are shown in Supporting Information Figure S3. This explains why the  $QA_{12}K^{2+}$  peptide, which is only 30% helical, is able to form a b<sub>12</sub> ion that is 54% helical. Simulations are therefore in excellent agreement with the experimental data, as the helical product is observed to form when proton transfer is unlikely and the more stable globular product is observed to form when proton transfer is more likely. It should be noted that direct deprotonation of the oxazolone by the N-terminus is reasonable due to the similarity of the basicities of the oxazolone nitrogen and N-terminus. Because values have not been reported for this particular molecule, the oxazolone basicity was taken from a 2-phenyl-5-oxazolone (912 kJ/mol) and the N-terminus was estimated from the basicity of a GGG tripeptide (905 kJ/mol).<sup>61–63</sup>

In Figure 3, a direct trend is observed between the linearity of helical abundance as a function of b ion fragment length and the conformation of the precursor. One feature of this plot is that the relative abundance of the helical b ion populations in Figure 3 ( $NA_n$  and  $DA_n$ ) is relatively constant from b<sub>10</sub>–b<sub>13</sub> and plummets between the b<sub>10</sub> and b<sub>9</sub> ion. The stability of a b<sub>9</sub> helix can be invoked to partially explain this characteristic, as it is substantially less stable than a b<sub>10</sub> helix (see Table 2), with the b<sub>10</sub>  $\alpha$ -helix being comprised of two complete turns of the helix (see Table 1) and the b<sub>9</sub> helix being comprised of only a single full turn and a partial second turn. Indeed, the abundance of the helical b<sub>8</sub> ion ( $NA_7$  and  $DA_7$  systems) is greater than the abundance of the helical b<sub>9</sub> ion. However, were thermody-

namics the only factor, the abundance of the helical b<sub>8</sub> ion would be expected to be similar to that of the b<sub>10</sub> ion. Hence, the length likely also plays a role, particularly because the N-terminus and C-terminal oxazolone ring are separated by only 10 Å in the  $NA_7$  b<sub>8</sub> ion. This relatively short length may permit proton transfer via alternative mechanisms. In contrast to the helical  $NA_n$  and  $DA_n$  b ions, the relative abundance of the helical  $QA_n$  b ions decreases linearly with decreasing fragment length. Consideration of the  $QA_{12}K^{2+}$  precursor, which is 90% globular, lends insight into this difference. Formation of b ions from globular conformations is predicted to yield b ions with relatively compact geometries, but initially protonated on the C-terminal oxazolone. If proton transfer to the N-terminus occurs, a stable globule will form. In the absence of proton transfer, the peptide will have time to fold into an oxazolone-protonated helix. The probability of proton transfer in a compact molecule is dependent on the probability that any given molecule is in a compact conformation conducive to proton transfer, either via backbone shuttling or a direct interaction between the N and C-termini. The probability function for proton transfer from the C-terminus to the N-terminus for a fragment of a particular length can be estimated by the sum of all conformations that permit proton transfer divided by the sum of all available conformations. A tremendous variety of compact geometries exists, especially compared to the number of linear geometries available. The addition of each amino acid to the fragment substantially increases the available number of compact geometries available because of conformational flexibility. Direct hydrogen bonding interactions between the N-terminus and C-terminal oxazolone ring can only occur from a handful of orientations, however, such as a coiled coil, a noncovalent macrocycle, or through an antiparallel beta-sheet type structure. Increasing the length of the peptide fragment is not expected to significantly increase the number of geometries in which the N and C-termini directly interact. Therefore, with increasing fragment length, the denominator, the total available compact conformations dramatically increases, while the numerator only moderately increases. As a consequence, the probability of proton transfer decreases with increasing fragment length, resulting in an increased abundance of the helical b ion structure.

In the higher collision energy regime, understanding b ion conformation becomes more complicated because a third process, dissociation of the b ion, can also occur. All secondary structures are also likely to be “melted” at such energies. As the collision energy is increased, the internal energy of the precursor and fragment ions are increased, causing the fragment ions to sample more conformational space. Thus, conformations favorable to direct proton transfer are more likely to be sampled. The termini of the helices are also more likely to fray or melt at higher collision energies, which may provide access to conformations that permit additional proton transfer pathways. All b ions containing a polar residue at the N-terminus form an equilibrium distribution of helical and globular conformers ( $\approx 20:80$ ) at high collision energies. The abundance of the helical  $LA_n$  b ions at high collision energies, in contrast, is characterized by a length dependence that is similar to the behavior of the peptide at low collision energies (see Figure 3). Because the leucine side chain is apolar while the Asp, Asn, and Gln side chains are able to hydrogen bond, the N-terminus and C-terminus likely must directly interact in the  $LA_n$  b ions in order for the charging proton to be transferred via direct hydrogen bond interactions. In contrast, the b ion

fragments with a polar N-terminal residue can presumably use the side chain of that residue to aid in shuttling the charging proton, increasing the number of pathways by which the proton can be transferred.

## CONCLUSIONS

Using IM-MS, four  $XA_nK^{2+}$  peptide analogues are shown to have both  $\alpha$ -helical and globular conformations, the relative abundance of which is seen to vary with the identity of the first amino acid and the length of the peptide. In particular, the  $DA_nK^{2+}$  peptide is observed to be comprised of a dominant  $\alpha$ -helical population while the  $QA_nK^{2+}$  peptide forms a dominant globular species, which follows the established solution phase trend for helical stability imparted by capping amino acids ( $D > N > Q$ ). These results mimic the trends found in solution phase studies, where aspartic acid provided the most stabilizing capping effects and glutamine was found to stabilize a nonhelical structure. Interestingly, we observe less stabilization when a hydrophobic residue, leucine, is used at the N-terminal capping amino acid, than the hydrogen-bonding residues aspartic acid and asparagine.

The b ion fragments of the  $XA_{12}K^{2+}$  species are shown to have both globular and helical conformations, and the relative abundance of these conformations is observed to vary as a function of the collision energy used to generate these fragments. The relative abundance of the helical and globular conformations are also observed to vary with the identity of the first amino acid and length of the fragment. These peptide fragments are observed to exist as different populations of structures at lower and higher collision energies, which is attributed to faster rates of proton transfer at higher energies due to increased conformational sampling. A connection between precursor conformation and b ion conformation appears to exist at low energies, as the peptides with the largest helical populations form b ions with the largest helical populations. However, as some globular precursors appear to form helical b ions, this relationship is skewed in favor of helical b ions stabilized by an oxazolone protonated C-terminus. However, the relative abundance of the helical b ion population diminishes for b ions smaller than the  $b_{10}$ , suggesting that abundant helical secondary structures in b ions are favored in helices with at least two full turns, e.g., the  $b_{10}$  and larger. Finally, the abundance of these secondary structures can be changed by merely varying the identity of the N-terminal capping residue, suggesting that the amino acid composition of N-terminal capping group on a peptide plays a significant role in the stabilization of helical secondary structures in gas phase peptides and their fragment ions.

## ASSOCIATED CONTENT

### Supporting Information

Figures S1–S3. This material is available free of charge via the Internet at <http://pubs.acs.org>.

## AUTHOR INFORMATION

### Corresponding Author

wysocki.11@osu.edu

### Notes

The authors declare no competing financial interest.

## ACKNOWLEDGMENTS

The Ohio Supercomputing Center is acknowledged for use of the supercomputers for the ab initio modeling. Dr. Marco Sotomayor is also thanked for all of his assistance with the NAMD software. We thank the reviewers for helpful suggestions that improved the paper. This research was supported by the National Science Foundation, grant DBI-0923551.

## REFERENCES

- (1) Dreveny, I.; Deeves, S. E.; Fulton, J.; Yue, B.; Messmer, M.; Bhattacharya, A.; Collins, H. M.; Heery, D. M. *Nucleic Acids Res.* **2014**, *42*, 822.
- (2) Sun, M.; Liu, J.; Qi, J.; Tefsen, B.; Shi, Y.; Yan, J.; Gao, G. F. *J. Immunol.* **2014**, *192*, 5509.
- (3) Padmanabhan, S.; Marqusee, S.; Ridgeway, T.; Laue, T. M.; Baldwin, R. L. *Nature* **1990**, *344*, 268.
- (4) Marqusee, S.; Robbins, V. H.; Baldwin, R. L. *Proc. Natl. Acad. Sci. U. S. A.* **1989**, *86*, 5286.
- (5) Merutka, G.; Shalongo, W.; Stellwagen, E. *Biochemistry* **1991**, *30*, 4245.
- (6) DeGrado, W. F.; Lear, J. D. *J. Am. Chem. Soc.* **1985**, *107*, 7684.
- (7) Kohtani, M.; Jarrold, M. F. *J. Am. Chem. Soc.* **2004**, *126*, 8454.
- (8) Kohtani, M.; Jones, T. C.; Schneider, J. E.; Jarrold, M. F. *J. Am. Chem. Soc.* **2004**, *126*, 7420.
- (9) Kohtani, M.; Jones, T. C.; Sudha, R.; Jarrold, M. F. *J. Am. Chem. Soc.* **2006**, *128*, 7193.
- (10) Kohtani, M.; Schneider, J. E.; Jones, T. C.; Jarrold, M. F. *J. Am. Chem. Soc.* **2004**, *126*, 16981.
- (11) Zilch, L.; Kaleta, D.; Kohtani, M.; Krishnan, R.; Jarrold, M. J. *Am. Soc. Mass Spectrom.* **2007**, *18*, 1239.
- (12) Ponomarev, S. Y.; Sa, Q.; Kaminski, G. A. *J. Chem. Theory Comput.* **2012**, *8*, 4691.
- (13) Kohtani, M.; Jones, T. C.; Sudha, R.; Jarrold, M. F. *J. Am. Chem. Soc.* **2006**, *128*, 7193.
- (14) Kohtani, M.; Schneider, J. E.; Jones, T. C.; Jarrold, M. F. *J. Am. Chem. Soc.* **2004**, *126*, 16981.
- (15) Mesleh, M. F.; Hunter, J. M.; Shvartsburg, A. A.; Schatz, G. C.; Jarrold, M. F. *J. Phys. Chem.* **1996**, *100*, 16082.
- (16) Bush, M. F.; Campuzano, I. D. G.; Robinson, C. V. *Anal. Chem. (Washington, DC, U. S.)* **2012**, *84*, 7124.
- (17) Bush, M. F.; Hall, Z.; Giles, K.; Hoyes, J.; Robinson, C. V.; Ruotolo, B. T. *Anal. Chem. (Washington, DC, U. S.)* **2010**, *82*, 9557.
- (18) Salbo, R.; Bush, M. F.; Naver, H.; Campuzano, I.; Robinson, C. V.; Pettersson, I.; Jorgensen, T. J. D.; Haselmann, K. F. *Rapid Commun. Mass Spectrom.* **2012**, *26*, 1181.
- (19) Campuzano, I.; Bush, M. F.; Robinson, C. V.; Beaumont, C.; Richardson, K.; Kim, H.; Kim, H. I. *Anal. Chem. (Washington, DC, U. S.)* **2012**, *84*, 1026.
- (20) Hopper, J. T. S.; Yu, Y. T.-C.; Li, D.; Raymond, A.; Bostock, M.; Liko, I.; Mikhailov, V.; Laganowsky, A.; Benesch, J. L. P.; Caffrey, M.; Nietlispach, D.; Robinson, C. V. *Nat. Methods* **2013**, *10*, 1206.
- (21) Florance, H. V.; Stopford, A. P.; Kalapothakis, J. M.; McCullough, B. J.; Bretherick, A.; Barran, P. E. *Analyst* **2011**, *136*, 3446.
- (22) O'Neil, K.; DeGrado, W. *Science* **1990**, *250*, 646.
- (23) Levitt, M. *Biochemistry* **1978**, *17*, 4277.
- (24) Aurora, R.; Rose, G. D. *Protein Sci.* **1998**, *7*, 21.
- (25) Doig, A. J.; Baldwin, R. L. *Protein Sci.* **1995**, *4*, 1325.
- (26) Doig, A. J.; Macarthur, M. W.; Stapley, B. J.; Thornton, J. M. *Protein Sci.* **1997**, *6*, 147.
- (27) Chakrabarty, A.; Doig, A. J.; Baldwin, R. L. *Proc. Natl. Acad. Sci. U. S. A.* **1993**, *90*, 11332.
- (28) Penel, S.; Hughes, E.; Doig, A. J. *J. Mol. Biol.* **1999**, *287*, 127.
- (29) Seale, J. W.; Srinivasan, R.; Rose, G. D. *Protein Sci.* **1994**, *3*, 1741.
- (30) Kumar, S.; Bansal, M. *Proteins: Struct., Funct., Genet.* **1998**, *31*, 460.

- (31) Lyu, P. C.; Wemmer, D. E.; Zhou, H. X.; Pinker, R. J.; Kallenbach, N. R. *Biochem.* **1993**, *32*, 421.
- (32) Forood, B.; Feliciano, E. J.; Nambiar, K. P. *Proc. Natl. Acad. Sci. U. S. A.* **1993**, *90*, 838.
- (33) Richardson, J.; Richardson, D. *Science* **1988**, *240*, 1648.
- (34) Morrison, L.; Somogyi, Á.; Wysocki, V. H. *Int. J. Mass Spectrom.* **2012**, *325–327*, 139.
- (35) Gucinski, A. C.; Chamot-Rooke, J.; Nicol, E.; Somogyi, A.; Wysocki, V. H. *J. Phys. Chem. A* **2012**, *116*, 4296.
- (36) Bush, M. F.; Campuzano, I. D.; Robinson, C. V. *Anal. Chem.* **2012**, *84*, 7124.
- (37) Phillips, J. C.; Braun, R.; Wang, W.; Gumbart, J.; Tajkhorshid, E.; Villa, E.; Chipot, C.; Skeel, R. D.; Kale, L.; Schulten, K. *J. Comput. Chem.* **2005**, *26*, 1781.
- (38) Frisch, M. J.; Trucks, G. W.; Schlegel, H. B.; Scuseria, G. E.; Robb, M. A.; Cheeseman, J. R.; Scalmani, G.; Barone, V.; Mennucci, B.; Petersson, G. A.; Nakatsuji, H.; Caricato, M.; Li, X.; Hratchian, H. P.; Izmaylov, A. F.; Bloino, J.; Zheng, G.; Sonnenberg, J. L.; Hada, M.; Ehara, M.; Toyota, K.; Fukuda, R.; Hasegawa, J.; Ishida, M.; Nakajima, T.; Honda, Y.; Kitao, O.; Nakai, H.; Vreven, T.; Montgomery, J. A., Jr.; Peralta, J. E.; Ogliaro, F.; Bearpark, M.; Heyd, J. J.; Brothers, E.; Kudin, K. N.; Staroverov, V. N.; Kobayashi, R.; Normand, J.; Raghavachari, K.; Rendell, A.; Burant, J. C.; Iyengar, S. S.; Tomasi, J.; Cossi, M.; Rega, N.; Millam, N. J.; Klene, M.; Knox, J. E.; Cross, J. B.; Bakken, V.; Adamo, C.; Jaramillo, J.; Gomperts, R.; Stratmann, R. E.; Yazyev, O.; Austin, A. J.; Cammi, R.; Pomelli, C.; Ochterski, J. W.; Martin, R. L.; Morokuma, K.; Zakrzewski, V. G.; Voth, G. A.; Salvador, P.; Dannenberg, J. J.; Dapprich, S.; Daniels, A. D.; Farkas, Ö.; Foresman, J. B.; Ortiz, J. V.; Cioslowski, J.; Fox, D. J. *Gaussian 09*; Gaussian, Inc.: Wallingford, CT, 2009.
- (39) Shvartsburg, A. A.; Jarrold, M. F. *Chem. Phys. Lett.* **1996**, *261*, 86.
- (40) Hudgins, R. R.; Ratner, M. A.; Jarrold, M. F. *J. Am. Chem. Soc.* **1998**, *120*, 12974.
- (41) Kohtani, M.; Jones, T. C.; Schneider, J. E.; Jarrold, M. F. *J. Am. Chem. Soc.* **2004**, *126*, 7420.
- (42) Harrison, A. G.; Young, A. B. *J. Am. Soc. Mass Spectrom.* **2004**, *15*, 1810.
- (43) Nold, M. J.; Wesdemiotis, C.; Yalcin, T.; Harrison, A. G. *Int. J. Mass Spectrom. Ion Processes* **1997**, *164*, 137.
- (44) Paizs, B.; Suhai, S. *Mass Spectrom. Rev.* **2005**, 508.
- (45) Polfer, N. C.; Oomens, J.; Suhai, S.; Paizs, B. *J. Am. Chem. Soc.* **2005**, *127*, 17154.
- (46) Zou, S.; Oomens, J.; Polfer, N. C. *Int. J. Mass Spectrom.* **2012**, *316–318*, 12.
- (47) Chen, X.; Yu, L.; Steill, J. D.; Oomens, J.; Polfer, N. C. *J. Am. Chem. Soc.* **2009**, *131*, 18272.
- (48) Wang, D.; Gulyuz, K.; Stedwell, C. N.; Yu, L.; Polfer, N. C. *Int. J. Mass Spectrom.* **2012**, *330–332*, 144.
- (49) Polfer, N.; Oomens, J.; Suhai, S.; Paizs, B. *J. Am. Chem. Soc.* **2007**, *129*, 5887.
- (50) Chen, X.; Steill, J. D.; Oomens, J.; Polfer, N. C. *J. Am. Soc. Mass Spectrom.* **2010**, *21*, 1313.
- (51) Perkins, B. R.; Chamot-Rooke, J.; Yoon, S. H.; Gucinski, A. C.; Somogyi, A.; Wysocki, V. H. *J. Am. Chem. Soc.* **2009**, 17528.
- (52) Arnott, D.; Kottmeier, D.; Yates, N.; Shabanowitz, J.; Hunt, D. F. *Proceedings of the 42nd ASMS Conference on Mass Spectrometry and Allied Topics*; American Society for Mass Spectrometry: Santa Fe, NM, 1994, p 470; May 29–June 3, 1994, Chicago, IL.
- (53) Zinnel, N. F.; Russell, D. H. *Anal. Chem.* **2014**, *86*, 4791.
- (54) Phillips, J. C.; Braun, R.; Wang, W.; Gumbart, J.; Tajkhorshid, E.; Villa, E.; Chipot, C.; Skeel, R. D.; Kale, L.; Schulten, K. *J. Comput. Chem.* **2005**, *26*, 1781.
- (55) Salbo, R.; Bush, M. F.; Naver, H.; Campuzano, I.; Robinson, C. V.; Pettersson, I.; Jorgensen, T. J.; Haselmann, K. F. *Rapid Commun. Mass Spectrom.* **2012**, *26*, 1181.
- (56) Wyttenbach, T.; Helden, G. v.; Batka, J. J., Jr.; Carlat, D.; Bowers, M. T. *J. Am. Soc. Mass Spectrom.* **1997**, *8*, 275.
- (57) Siu, C.-K.; Guo, Y.; Saminathan, I. S.; Hopkinson, A. C.; Siu, K. W. M. *J. Phys. Chem. B* **2009**, *114*, 1204.
- (58) Zakharova, N. L.; Crawford, C. L.; Hauck, B. C.; Quinton, J. K.; Seims, W. F.; Hill, H. H., Jr.; Clark, A. E. *J. Am. Soc. Mass Spectrom.* **2012**, *23*, 792.
- (59) Badman, E. R.; Hoaglund-Hyzer, C. S.; Clemmer, D. E. *J. Am. Soc. Mass Spectrom.* **2002**, *13*, 719.
- (60) Pierson, N. A.; Valentine, S. J.; Clemmer, D. E. *The Journal of Physical Chemistry B* **2010**, *114*, 7777.
- (61) Hunter, E. P. L.; Lias, S. G. *J. Phys. Chem. Ref. Data* **1998**, *27*, 413.
- (62) Nold, M. J.; Cerda, B. A.; Wesdemiotis, C. *J. Am. Soc. Mass Spectrom.* **1999**, *10*, 1.
- (63) Rodriguez, C. F.; Cunje, A.; Shoeib, T.; Chu, I. K.; Hopkinson, A. C.; Siu, K. W. M. *J. Am. Chem. Soc.* **2001**, *123*, 3006.